COMMUNICATION

Check for updates

Bioresponsive microlasers with tunable lasing wavelength†

Zhiyi Yuan,[a] Xiaotian Tan, [b] Xuerui Gong,[a] Chaoyang Gong,[a] Xin Cheng,[a] Shilun Feng,[c] Xudong Fan [b] and Yu-Cheng Chen ⋆[a,d]

Lasing particles are emerging tools for amplifying light–matter interactions at the biointerface by exploiting its strong intensity and miniaturized size. Recent advances in implementing laser particles into living cells and tissues have opened a new frontier in biological imaging, monitoring, and tracking. Despite remarkable progress in micro- and nanolasers, lasing particles with surface functionality remain challenging due to the low mode-volume while maintaining a high *Q*-factor. Herein, we report the novel concept of bioresponsive microlasers by exploiting interfacial energy transfer based on whispering-gallery-mode (WGM) microdroplet cavities. Lasing wavelengths were manipulated by energy transfer-induced changes of a gain spectrum resulting from the binding molecular concentrations at the cavity surface. Both protein-based and enzymatic-based interactions were demonstrated, shedding light on the development of functional microlasers. Finally, tunable lasing wavelengths over a broad spectral range were achieved by selecting different donor/acceptor pairs. This study not only opens new avenues for biodetection, but also provides deep insights into how molecules modulate laser light at the biointerface, laying the foundation for the development of smart bio-photonic devices at the molecular level.

1. Introduction

Since the first invention of lasers six decades ago, lasers have advanced rapidly from fundamental physics to modern technologies. An emerging class of lasers named biological lasers, which utilize biological analytes or biological related

[a]*School of Electrical and Electronic Engineering, Nanyang Technological University, 50 Nanyang Avenue, 639798, Singapore. E-mail: yucchen@ntu.edu.sg*
[b]*Department of Biomedical Engineering, University of Michigan, Ann Arbor, 1101 Beal Ave., Ann Arbor, MI, 48109, USA*
[c]*State Key Laboratory of Transducer Technology, Shanghai Institute of Microsystem and Information Technology, Chinese Academy of Sciences, Shanghai, 200050, China*
[d]*School of Chemical and Biomedical Engineering, Nanyang Technological University, 62 Nanyang Drive, 637459, Singapore*
†Electronic supplementary information (ESI) available. See DOI: 10.1039/d0nr07921a

materials as the gain medium, has shown promising potential in biomedical applications.[1–6] Laser emission-based detection offers distinct advantages in terms of signal amplification, narrow linewidth, and strong light–matter interactions.[4,7–12] The remarkably narrow linewidth of the lasing spectrum further enhances the capability for multiplexing.[7,13–16] Recently, several types of active resonators have been employed as lasing particles,[17–19] including Fabry–Pérot-based nanowires,[20,21] plasmonic nanolasers,[6] and whispering-gallery-mode (WGM) microspheres.[15,22–29] In particular, WGM microlaser particles are attractive candidates for sensing at the biointerface, due to its high-*Q* factor, miniaturized size, and potential for cellular and molecular analysis. For instance, WGM lasers have been recently integrated into living cells and tissues, opening a new frontier in biological imaging, monitoring, and tracking.[7,24,26,28,30,31] Nonetheless, the vast majority of lasing particles rely on the changes of refractive indexes, electrostatics, and surface physical properties to obtain sensing functions.

To overcome the limitations, here we report the concept of bioresponsive microlasers by exploiting the mechanism of interfacial energy transfer.[32] Lasing wavelengths were manipulated by the energy transfer-induced changes of the gain spectrum resulting from the binding molecular concentration. Fig. 1a illustrates the concept of a biofunctional microlaser, where the exceptionally high concentration of dyes (donor) inside the cavity triggers coherent-radiative energy transfer to excite biomolecules (acceptor) binding to the cavity interface. We surprisingly discovered that the lasing wavelength is determined by the acceptor/donor ratios (A/D) when different concentrations of acceptor molecules bind to the donor-droplet, contributing to different energy transfer efficiencies at the cavity interface. As presented in Fig. 1b, the fluorescence emission remains at a similar wavelength as the concentration of the binding analyte (A/D ratio) increases. However, a slight increase in the gain profile from the attached molecules enabled the distinguishable lasing wavelength to shift accordingly. The underlying principle of the bio-responsive laser is depicted in Fig. 1c. The pump laser energy can be harvested by
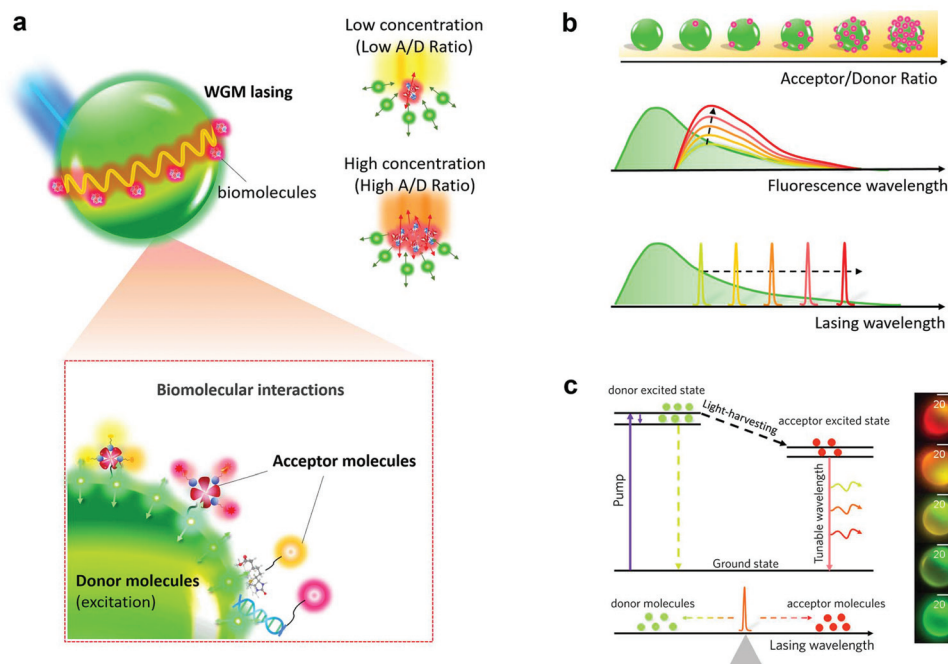
Fig. 1 (a) Top panel: Schematic diagram of the working principle of interfacial energy transfer laser. The substantial green droplet indicates the liquid crystal microcavity doped with donor dye, while the red particles represent acceptor molecules with fluorescence emitting binding biomolecules at the droplet surface. Different acceptor/donor (A/D) ratios will result in different interfacial energy transfer and thus laser emission wavelengths. Bottom panel: Principle illustrating the bio-responsive interfacial energy transfer laser, where donor and acceptor molecules are separated at the microcavity interface. Donor molecules will excite acceptor molecules to generate laser emissions at the interface upon biomolecular interactions. (b) Comparison between fluorescence sensing and the proposed interfacial lasing bioanalysis as the analyte concentration (A/D ratio) increases. Interfacial lasing wavelength appears redshifts as the analyte concentration (A/D ratio) increases. (c) Schematic diagram of interfacial energy transfer laser. The black dash arrow represents the energy transfer between donor and acceptor molecules. The A/D ratio will affect the lasing wavelength owing to the resonance energy transfer efficiency and re-absorption in the stimulated emission process. The inset CCD shows the microlaser doped with Coumarin 6 by adding different concentrations of Rhodamine 6G (A: acceptor, D: donor).

the donor to generate excited state molecules and transfer to the acceptor through resonance energy transfer. The efficiency of the resonance energy transfer and re-absorption in the stimulated emission process will thus affect the output lasing wavelengths. For instance, the CCD images of microlaser emission corresponding to different A/D ratios are shown in Fig. 1c, changing from green to red. Simulations and experiments also support the concept where the A/D ratio plays a crucial role in modulating lasing wavelengths.

To demonstrate the potential of bioresponsive microlasers, specific bindings of biomolecules were investigated by functionalizing the surface of microdroplets. Different A/D ratios lead toward different wavelengths upon molecule binding. Microlaser particles were also demonstrated with various donor–acceptor pairs, generating lasing emissions over a wide range of wavelengths. Finally, we explored the possibility of tuning laser emissions with biochemical reactions, including protein-based and enzymatic-based reactions—narrow lasing wavelengths redshift as the reaction concentration or reaction time increases. The significance of this work represents a milestone to achieve microlaser particles with controllable functions, laying the foundation for tunable photonic devices and bio-integrated sensing by means of laser emissions.

2. Experiments and materials

Preparation of microdroplet cavities

To prepare dye doped liquid crystal (LC) microdroplets, 3.55 mg (10 μmol) of Coumarin 6 or 3.24 mg (10 μmol) of Bodipy or 3.18 mg (10 μmol) of Nile Red was added to 500 μL of 5CB LC and then mixed by vortexing for 10 minutes. The final dye concentration in the LC is 20 mM. For preparing the LC microdroplet aqueous solution, 28.8 mg (0.1 mol) of SDS was added to 50 mL of PBS solution. The mixture was stirred magnetically for about 20 minutes at 1000 rpm to obtain a homogeneous SDS/PBS solution. To prepare the LC microdroplet emulsion, 10 μL of dye doped LC was added to 1 mL of homogeneous SDS/PBS solution. The resulting mixture was mixed by vortex for 1 minute to produce LC microdroplet emulsion. For all the laser experiments in this work, a predefined droplet size of 28 ± 2 μm was used.

Fixing microdroplets onto glass slides

For the glass slides, we first cleaned the glass slides using acetone before applying 2% v/v APTES/acetone for a period of 3 min. Then, we washed the slides with ethanol two times and washed them with water. Next, we dried the slides at 25 °C for

12 h. To obtain the solution, we added 30 mg (260 µmol) of NHS and 30 mg (156 µmol) of EDC into 5 mL of PBS solution and put glass slides into solution; we then added the solution to a Petri dish and placed the glass slides into the solution. To immobilize the LC microdroplets on APTES modified slide cover glasses, the carboxylic groups of LC microdroplets were activated by adding LC microdroplet emulsion into the Petri dish, which contained NHS and EDC dissolved PBS solution. Finally, the Petri-dishes were stored at room temperature for 12 hours.[33]

Preparation of PLL-modified or streptavidin (SA) coated LC microdroplets

First, 5CB microdroplets (10 µL) were prepared in the 1 mL SDS/PBS solution and subjected to sonication for 5 min. Second, the solution was replaced by 0.01% poly-L-lysine (PLL) solution following centrifugation at 5000 rpm for 4 min. Here, PLL was used to fix the droplets due to the positively charged property. Then, we incubated the product at room temperature for 30 min.[34] Following incubation, the LC microdroplets were washed by adding PBS solution and performing centrifugation. Regarding the streptavidin (SA)-coating process, 500 µL of SA/PBS solution with a 0.1 mg mL^{-1} concentration was added to LC microdroplets before it was subjected to slow mixing for a period of 1 h. Finally, the microdroplets were washed with PBS solution twice to remove the unbound SA in the surrounding medium. To prepare the dye-labeled biotin incubated LC microdroplet, we applied SA coated LC microdroplets into the different concentrations of dye-labeled biotin/PBS solution for 1 hour. For specific binding on the microdroplet surface, droplets were washed with PBS solution to remove unbound dye-labeled biotin in the surrounding medium.

Preparation of LC microdroplets for enzymatic reactions

To prepare suitable dye doped LC microdroplets, we chose Bodipy for the donor inside the LC microdroplet, and the final dye concentration in the LC is 20 mM. For the blocking process, we added 500 µL of BSA/PBS solution with a concentration of 10 mg mL^{-1} to the SA coated LC microdroplets after the washing process; this was used to prevent non-specific protein binding. Following 30 minutes of incubation, LC microdroplets were washed with PBS solution and centrifugation. Then, the biotin-HRP diluted to different concentrations was added to the LC microdroplets and incubated for 1 hour. The microdroplets were then washed with PBS solution twice to remove the unbound biotin-HRP in the surrounding medium. The working substrate solution was prepared based on the manufacturer's manual at room temperature. The ratio of three substrate components, QuantaRed ADHP concentrate : QuantaRed enhancer solution : QuantaRed stable peroxide solution = 1 : 10 : 10. For enzymatic-reaction characterization, we mixed LC microdroplets and enzyme–substrate solution with a ratio of 4 : 6 on the glass slide for one reaction site, which was optically pumped with the pulse laser. For the identical biotin-HRP concentration, several reaction sites with different beginning times could be measured on one glass slide.

Optical system setup

For the excitation of the LC microdroplet and the collection of laser emission, an inverted microscopic system (Nikon Ti2) with a 20× 0.4 NA objective was used. Optical pumping was achieved using a pulsed ns-laser (EKSPLA PS8001DR) integrated with an optical parametric oscillator with a repetition rate of 50 Hz and a pulse duration of 5 ns. According to the respective absorption wavelength of fluorophores, the pump laser was tuned to 450 nm for Coumarin 6, 488 nm for Bodipy, 532 nm for Nile Red. The beam diameter at the objective focal plane was ∼16 µm wide. The collected light was sent into a charge-coupled device camera or an imaging spectrometer (Andor Kymera 328i and Newton 970 EMCCD). For measurements of the fluorescence image, an integrated LED was used as the excitation source and imaged using a color CCD (Basler acA1600-20uc) mounted on the inverted microscope.

Materials and chemicals

The dyes used in this study were purchased from Sigma Aldrich, Tokyo Chemical Industry, and Thermo Fisher Scientific, including Coumarin 6 (C6) (Sigma-Aldrich #442631), 1,3,5,7-tetramethyl-8-phenyl-4,4-difluoroboradiazaindacene (Bodipy) (Sigma-Aldrich #793728), Rhodamine 6G (R6G) (Sigma-Aldrich #83697), Streptavidin Alexa Fluor 514 conjugate (Thermo Fisher Scientific #S32353), Streptavidin (Tokyo Chemical Industry #S0951), Atto 520-Biotin (Biotin 520) (Sigma-Aldrich #01632), Atto 550-Biotin (Biotin 550) (Sigma-Aldrich #28923), Atto 590-Biotin (Biotin 590 M_w, 1001.62 g mol^{-1}) (Sigma-Aldrich #43208), and Atto 655-Biotin (Biotin 655) (Sigma-Aldrich #06966). The chemical (3-aminopropyl)triethoxysilane (APTES) we used for glass cover slides saline coupling modified was purchased from Tokyo Chemical Industry (#A0439) (M_w, 221.37 g mol^{-1}). For preparation of liquid crystal droplets, 4-cyano-4′-pentylbiphenyl purchased from Tokyo Chemical Industry (#C1550) as the nematic liquid crystal (5CB) and sodium dodecyl sulfate (SDS) (Sigma-Aldrich #L3771) as the surfactant. N-Hydroxysuccinimide (NHS) (Sigma-Aldrich#130672) and N-(3-dimethylaminopropyl)-N-ethylcarbodiimide hydrochloride (EDC) were purchased from Sigma Aldrich (Sigma-Aldrich #03450). For the surface modified LC microdroplet, we used the poly-L-lysine solution (PLL M_w, 150 000–300 000 g mol^{-1}) which was purchased from Sigma Aldrich (#P4832). Bovine serum albumin (BSA) was purchased from Sigma Aldrich (#P5396) as a surface blocking buffer. Biotinylated peroxidase (biotin-HRP) was purchased from Thermo Fisher Scientific (#432040). The chemifluorescent substrate (QuantaRed Enhanced Chemifluorescent HRP Substrate Kit) was purchased from Thermo Fisher Scientific (#15159). The microwell array used in the previous section was purchased from Microsurface (#MGA-050-01), AU.

3. Results

In this study, lasing particles were formed by taking advantage of WGM microcavities composed of nematic liquid crystals.[35]

The WGM cavity relies on the total internal reflection at the droplet interface to provide optical feedback. Fig. S1a† plots the electric field distribution in 10 μm diameter microsphere, showing the symmetrical electric field distribution. As a proof-of-concept, lasing was conducted by using a fixed Coumarin 6 (C6) microdroplet by applying Rhodamine 6G (R6G) molecules to the cavity interface as shown in Fig. 2. Interfacial lasing based on coherent-radiative energy transfer was therefore generated. We first investigated the role of coherent-radiative energy transfer and nonradiative Förster resonance energy transfer (FRET) by conducting time-resolved fluorescence lifetime measurements in Fig. S1b.† The donor lifetime, in the absence and presence of an acceptor, is 2.08 ns and 2.05 ns, respectively. The extremely low FRET efficiency (∼1.5%) shows that radiative energy transfer plays a dominant role in such an interfacial laser. As a control group, Fig. S2† confirms that the lasing from R6G originates from the cavity energy transfer from the C6-donor (not from direct 450 nm pump excitation). It is noted that almost all the obvious peaks are the transverse magnetic (TM) mode. The reason for this phenomenon is due to the fact that the TM modes possess higher refractive index contrast than the transverse electric (TE) modes in the radial LC microdroplet. Normally, TM modes and TE modes in WGM polarizations correspond to the electric field oscillating in parallel and perpendicular to radial orientation, respectively.[36] Besides, the parallel and perpendicular to radial orientation denote the extraordinary and ordinary refractive index in the radial LC microdroplet, in which the extraordinary refractive index is higher than the ordinary refractive index. According to WGM theory, the free spectral range (FSR) can be calculated using the formula: $FSR = \lambda^2/n_{eff}.\pi D$, where λ is the wavelength, $n_{eff.}$ is the effective refractive index, and D is the WGM cavity diameter. To emphasize the effect of cavity energy transfer, we compared the lasing threshold of R6G molecules excited by the emission from C6 donor-droplet and excited directly by using a 532 nm laser beam (Fig. 2a). At a fixed R6G concentration, Fig. 2b and c presented significantly higher lasing intensity and lower lasing threshold with the existence of the donor-droplet, indicating the critical role of the donor-droplet. By changing the C6-donor concentration in the droplet (with fixed acceptor concentration), the lasing wavelength shows a redshift as the A/D ratio increases (Fig. S3a†). The required lasing threshold for the respective C6-donor concentration to achieve interfacial lasing was also studied (Fig. S3b†), demonstrating the significance of the donor-droplet.

Next, we explored the lasing spectra at various A/D ratios when different concentrations of acceptor molecules bind to the surface of the donor droplet (fixed concentration) in Fig. 2d. As one can see, the original lasing from the microdroplet (C6, donor) is located at 538 nm (A/D = 0). The lasing wavelength starts to redshift as we increased the analyte (R6G, acceptor) concentration, resulting from A/D = 0.00025 to A/D = 0.0375. At lower A/D ratios, fewer molecules were excited; thus, a smaller redshift was obtained. At higher A/D ratios, a huge amount of R6G molecules binding the droplet were excited, hence generating lasing at longer wavelengths. Fig. 2e demonstrates the relationship between the lasing peak wavelength (560 nm to 630 nm) and energy transfer ratios (A/D) extracted from Fig. 2d. The slope of the fitted line (wavelength shifting rate) becomes lower at relatively high A/D due to the saturation
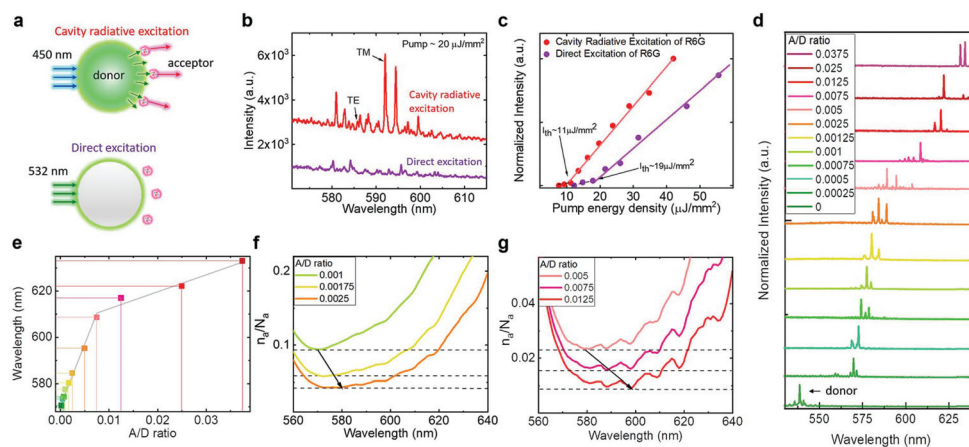
Fig. 2 (a) Schematic diagram of cavity radiative excitation of Rhodamine 6G (R6G) and direct excitation of R6G. The highly concentrated Coumarin 6 (C6) acts like a light-harvesting antenna to excite a low concentration of acceptor molecules. The red particles represent the acceptor molecules (R6G). (b) Lasing spectra of R6G under cavity radiative excitation (A/D = 0.005) and direct excitation at a relatively low pump energy density; the curves have been vertically shifted for clarity. (c) Spectrally integrated laser output as a function of pump energy density, and the solid line denotes a linear fit; the lasing threshold is approximately 11 μJ mm^{-2} and 19 μJ mm^{-2}. Red line and violet line represent the cavity radiative excitation (light-harvesting excitation) and direct excitation, respectively. (d) Lasing spectra of the Coumarin 6 (C6) microdroplet with various analyte concentrations (A/D ratio); the curves have been vertically shifted for clarity, and the background fluorescence has been subtracted from the spectra. (e) Lasing output wavelength as a function of the A/D ratio extracted from the spectra in (d), the solid lines are the linear fit. (f and g) The fraction of R6G molecules in the first excited states needed at the laser threshold for various representative R6G concentrations based on eqn (3). As the A/D ratio increases, the wavelength which requires minimum excited molecules fraction appears red shifted. Diameter of droplet = 28 μm. Donor-droplet concentration = 20 mM. The A/D ratio represents the acceptor concentration/donor concentration.

of molecules on the microdroplet surface. To elucidate the underlying mechanisms for the redshift of laser emissions, we carried out the laser rate equations based on acceptor molecules in eqn (1):

$$\frac{dq_a}{dt} = \frac{n_a c q_a}{m}\sigma_e(\lambda) - \frac{(N_a - n_a)c q_a}{m}\sigma_a(\lambda) - \frac{q_a}{\tau_{cavity}}, \quad (1)$$

where N_a is the total concentration of acceptor molecules, and n_a is the concentration of excited state acceptor molecules. $\sigma_e(\lambda)$ and $\sigma_a(\lambda)$ are the acceptor emission and absorption cross-sections. q_a is the acceptor emitted photon number density in the cavity. τ_{cavity} is the lifetime of the photons in the cavity which is equal to $\eta Q\lambda/2\pi c$. m and c represent the refractive index of the surrounding medium (~1.33) and light speed in the vacuum. η means the fraction of mode energy in the evanescent field. Under steady-state conditions, we can obtain eqn (2):

$$n_a\sigma_e(\lambda) - (N_a - n_a)\sigma_a(\lambda) - \frac{2\pi m}{\lambda\eta Q} = 0, \quad (2)$$

From eqn (2), we can derive the fraction of acceptor molecules at the excited state under the threshold condition:[19]

$$\gamma_{th} = \frac{n_a}{N_a} = \frac{1}{\sigma_e(\lambda) + \sigma_a(\lambda)}\left[\sigma_a(\lambda) + \frac{2\pi m}{N_a\lambda\eta Q}\right], \quad (3)$$

According to eqn (3), different R6G acceptor concentrations (A/D ratios) will give rise to γth values at respective wavelengths. Fig. 2f and g plots the γ_{th} values for various A/D ratios

based on eqn (2), in which the quality factor (Q) is equal to 5×10^5 and η is equal to 0.1.[35]

The dashed curves in Fig. 2f and g represent the fraction of acceptor molecules at the excited state at fixed pump energy density. When the pump energy reaches a specific molecule fraction (γ_{th}), lasing will start to emerge at a particular wavelength (the lowest point in the curve). According to the simulation results, the wavelength corresponding to the minimum fractional acceptor molecules redshifts as the acceptor concentration increases around the cavity surface. The above equations did not consider the effect of donor molecules in the interfacial laser. As such, we also calculated the lasing wavelength based on the different A/D ratios after we consider the effect of donor molecules (ESI Note 1† section 1). Fig. S3c† plots the γ_{th} values for various A/D ratios (various donor concentrations). The lasing wavelength blue shifts as the donor concentration increases (A/D ratio decreases). The overall trend of simulation results is in good agreement with the experimental results for A/D ratios. However, owing to the competition between various modes, this model is not sufficient when the pump energy is far beyond the lasing threshold.

By labeling target biomolecules with suitable fluorophores, a similar concept can be applied to different molecular interactions. As such, in the following sections, we systematically demonstrated how protein-based and enzymatic-based interactions could adjust the lasing wavelengths. In Fig. 3a, we show the design for protein-based interactions. Herein, a monolayer of streptavidin (SA) molecules was coated on the surface of the microdroplet. To prevent nonspecific bindings,
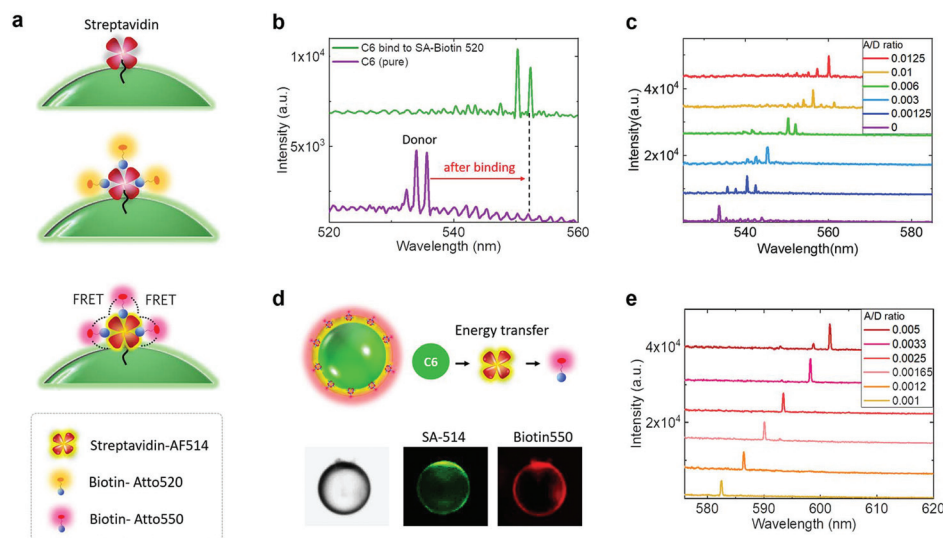

Fig. 3 (a) Schematic diagram of specific binding at the surface of the Coumarin 6 (C6) microdroplet. Streptavidin (SA) molecules were coated on the microdroplet surface (top configuration), and then biotin molecules were bound to SA (middle configuration). The bottom configuration shows the Streptavidin-Alexa Fluor 514 (SA-AF514) coated microdroplet binding with Atto 550-biotin (Biotin 550) incubation. (b) Violet line: lasing spectra of C6 microdroplet laser; green line: lasing spectra of surface-specific binding C6 microdroplet laser. (c) Lasing spectra of the C6 microdroplet with various Biotin 520 concentrations (A/D ratio). (d) Top: Schematic illustration of energy transfer from C6 to SA-AF514 and finally to Biotin 550; bottom: fluorescence image showing the binding of Biotin 550 and SA-AF514 on the plain LC microdroplet surface. (e) FRET lasing spectra of the SA-AF514 coated microdroplet when binding with different Biotin 550 concentrations (A/D ratio); the curves have been vertically shifted for clarity, and the background fluorescence has been subtracted from the spectra. Diameter of droplet = 28 μm.

blocking and washing steps have been conducted to ensure the binding event between SA and biotin molecules. As shown in Fig. 3a, laser emission is expected to change when biotin molecules (labeled with Atto520) bind to streptavidin. Fig. 3b presents the lasing spectra of C6 microdroplet coated with SA (green curve), before and after binding to Biotin 520 (purple curve). The enormous redshift is mainly due to the extremely high binding affinity between biotin and SA, therefore absorbing most of the energy (photons) emitted by C6. Based on the same concept, we investigated the lasing spectra at various A/D ratios, in which Biotin 520 serves as the acceptor, and the C6-droplet serves as the donor. As expected, the lasing peak redshifts as the A/D ratio increases, as shown in Fig. 3c, where a linear relationship was also found between the peak wavelength and biotin concentrations (Fig. S4a†). Fig. S5a† presents the laser emission spectra of Biotin 520 binding to SA (on LC microdroplets) at various pump energy densities, where Fig. S5b† shows a lasing threshold of 12 μJ mm^{-2}.

Moving a step forward, streptavidin labeled with AF514 (SA-AF514) and biotin-labeled with Atto550 (Biotin 550) were selected as donor and acceptor molecules, respectively. The bottom panel of Fig. 3a presents a schematic diagram of FRET interaction between SA-AF514 and Biotin 550 on the cavity surface. Fig. 3d shows that interfacial lasing could be generated when pump energy is absorbed by SA-AF514 and subsequently transferred to Biotin 550. To confirm the binding of

FRET interactions, the corresponding fluorescence microscopic images are shown in Fig. 3d as well. Fig. 3e presented the lasing spectra excited by SA-AF514 upon different A/D ratios. For droplets under predefined size and conditions, the lasing wavelength redshifts as the A/D ratios increase. Sharp lasing modes were observed due to relatively low spectral overlap between C6 emission and Biotin 550 absorption. A linear relationship between the peak wavelength and biotin concentrations was studied as shown in Fig. S4b.† In order to confirm FRET lasing, a microdroplet coated with pure SA was used as a control experiment. Fig. S6† shows the microdroplets coated with pure SA and binding with Biotin 550 on the cavity surface only. In Fig. S7,† we compared the lasing threshold between SA-AF514/Biotin 550 and pure-SA/Biotin 550 at the same pump wavelength. The lasing threshold for SA-AF514/Biotin 550 was two times lower than the direct excitation of SA/Biotin 550, demonstrating the existence of FRET.

Next, we further explore the possible implementation of interfacial microlaser in enzymatic reactions, as illustrated in Fig. 4a. The lasing wavelength is adjusted by the reaction time, which is the result of a different A/D ratio. As the product concentration increases with the reaction time, the A/D ratio increases, and hence the lasing wavelength redshifts accordingly. To validate our concept, a monolayer of SA molecules was coated on the microdroplet (BODIPY) and incubated with biotinylated peroxidase (biotin-HRP) after blocking with
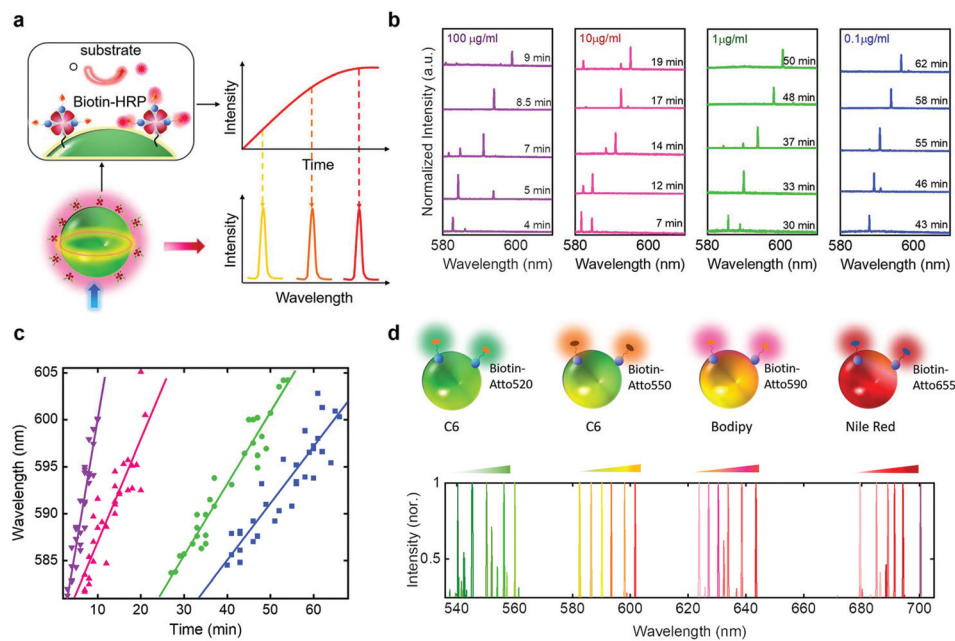
Fig. 4 (a) Conceptual illustration of enzymatic-responsive laser based on the interfacial laser. Enzyme–substrate reaction, which occurs at the surface of the microdroplet produces the fluorescent products acting as the interfacial laser gain medium. Lasing peak appears redshifted with time as the product concentration (A/D ratio) increases. (b) Reaction time-dependent enzymatic normalized lasing spectra by changing the biotin-HRP concentrations (0.1, 1, 10, and 100 μg ml^{-1}). (c) Statistics of lasing peak wavelength as a function of reaction time based on different biotin-HRP concentrations (0.1, 1, 10, and 100 μg ml^{-1}). (d) Top: Schematic diagram of 4 different microlasers originating from specifically designed donor/acceptor pairs: Coumarin 6 (C6) droplet with the Biotin 520 molecule; C6 droplet with the Biotin 550 molecule; Bodipy droplet with the Biotin 590 molecule; Nile Red (NR) droplet with the Biotin 655 molecule. Normalized laser emission spectra extracted from the four donor/acceptor pairs whereby different A/D ratios are applied. The color bar on top represents the increase of the A/D ratio for each droplet pair.

bovine serum albumin (BSA). Subsequently, enzyme–substrate solution was applied to the droplet. When binding between biotin-HRP and SA molecules occurs on the cavity surface, the reacted enzyme–substrate then serves as the interfacial laser gain medium (Fig. S8†). Herein, we first investigated the lasing spectra *versus* reaction time based on the same microdroplet in Fig. S9,† where the lasing spectrum was collected at different time slots. As expected, the lasing peak shifts to longer wavelengths as the reaction time increases (increased A/D ratio). Fig. 4b further shows the analysis of the time-dependent lasing spectra at different biotin-HRP concentrations (0.1, 1, 10, and 100 μg ml^{-1}). To further attest to the reproducibility of such discovery, a large number of data is provided in Fig. 4c. It was found that at higher biotin-HRP concentrations (higher A/D ratios), lasing peaks also shift faster due to accelerated substrate reaction rate, resulting in larger slope efficiency.

Finally, by choosing suitable donor/acceptor pairs that have spectral overlap between donor emission and acceptor absorption, the proposed interfacial laser could be achieved at desirable wavelengths. Shown in Fig. 4d are the schematic diagrams of the interfacial laser platform based on 4 different donor/acceptor combinations by separating at the cavity interface. The corresponding fluorescence emission/absorption spectra of various donor/acceptor pairs are plotted in Fig. S10.† Other details of the spectrum (laser and fluorescence) can be found in Fig. S11 and S12.† As a proof-of-concept, biotin molecules conjugated with different fluorophores were utilized as acceptor molecules in the four models. By varying the A/D ratios, the normalized laser emission spectra from four different donor/acceptor pairs are demonstrated in Fig. 4d. The selection and design of the donor/acceptor fluorophore also play a significant role in interfacial laser efficiency. The higher the overlap between the donor emission spectrum and acceptor absorption, the higher the energy transfer efficiency.

4. Discussion

In this study, we proposed a biological responsive microlaser particle in which the laser emission wavelengths are modulated by surface molecular interactions. Taking advantage of interfacial energy transfer at the cavity biointerface, the concentration ratios between the analytes (acceptor) and the droplet (donor) resulted in different lasing wavelengths. Both protein-based and enzymatic-based reactions were demonstrated. This work not only demonstrated the potential for laser-based detection but opens the roadmap to achieve bio-functional microlasers. In this work, we used the liquid crystal as the material of mircrodroplets owing to its biocompatible,[37] extraordinary processability,[38] and intriguing optoelectronic properties.[39] However, it is also noteworthy that the microdroplet material is not only limited to the liquid crystal but can be any biocompatible material that allows fluorophore doping inside to form the microlaser. By changing to higher refractive index materials, the required size to achieve lasing could also

become smaller and, therefore, will be more biocompatible for biological detection. Additionally, the improvement of the cavity *Q*-factor is also necessary to achieve better stability and precision control. In a nutshell, we envisage that this novel concept may deepen insights into how molecules interact with and modulate laser light, laying the foundation for the development of tunable photonic devices at the molecular level, such as highly selective laser devices, laser-emission imaging, and bio-inspired sensing.

Conflicts of interest

The authors declare no conflicts of interest.

Acknowledgements

References

1 X. Yang, W. Shu, Y. Wang, Y. Gong, C. Gong, Q. Chen, X. Tan, G.-D. Peng, X. Fan and Y.-J. Rao, Turbidimetric inhibition immunoassay revisited to enhance its sensitivity via an optofluidic laser, *Biosens. Bioelectron.*, 2019, **131**, 60–66.

2 X. Tan, Q. Chen, H. Zhu, S. Zhu, Y. Gong, X. Wu, Y.-C. Chen, X. Li, M. W.-H. Li and W. Liu, A Fast and Reproducible ELISA Laser Platform for Ultrasensitive Protein Quantification, *ACS Sens.*, 2019, **5**(1), 110–117.

3 J. E. Hales, G. Matmon, P. A. Dalby, J. M. Ward and G. Aeppli, Virus lasers for biological detection, *Nat. Commun.*, 2019, **10**(1), 1–11.

4 Y.-C. Chen, X. Tan, Q. Sun, Q. Chen, W. Wang and X. Fan, Laser-emission imaging of nuclear biomarkers for high-contrast cancer screening and immunodiagnosis, *Nat. Biomed. Eng.*, 2017, **1**(9), 724–735.

5 S. Cho, M. Humar, N. Martino and S. H. Yun, Laser Particle Stimulated Emission Microscopy, *Phys. Rev. Lett.*, 2016, **117**(19), 193902.

6 E. I. Galanzha, R. Weingold, D. A. Nedosekin, M. Sarimollaoglu, J. Nolan, W. Harrington, A. S. Kuchyanov, R. G. Parkhomenko, F. Watanabe, Z. Nima, A. S. Biris, A. I. Plekhanov, M. I. Stockman and V. P. Zharov, Spaser as a biological probe, *Nat. Commun.*, 2017, **8**, 15528.

7 N. Martino, S. J. J. Kwok, A. C. Liapis, S. Forward, H. Jang, H.-M. Kim, S. J. Wu, J. Wu, P. H. Dannenberg and S.-J. Jang, Wavelength-encoded laser particles for massively-multiplexed cell tagging, *Nat. Photonics*, 2019, (13), 720–727.

8 Y. C. Chen and X. Fan, Biological Lasers for Biomedical Applications, *Adv. Opt. Mater.*, 2019, **7**(11), 1900377.

9   Y.-C. Chen, Q. Chen and X. Fan, Lasing in blood, *Optica*, 2016, **3**(8), 809–815.

10 Z. Lv, Z. Man, Z. Xu, C. Feng, Y. Yang, Q. Liao, X. Wang, L. Zheng and H. Fu, Intracellular near-Infrared Microlaser Probes Based on Organic Microsphere–SiO2 Core–Shell Structures for Cell Tagging and Tracking, *ACS Appl. Mater. Interfaces*, 2018, **10**(39), 32981–32987.

11 X. Fan and S.-H. Yun, The potential of optofluidic biolasers, *Nat. Methods*, 2014, **11**, 141–147.

12 T. Watanabe, Y. Saijo, Y. Hasegawa, K. Watanabe, Y. Nishijima and T. Baba, Ion-sensitive photonic-crystal nanolaser sensors, *Opt. Express*, 2017, **25**(20), 24469–24479.

13 A. H. Fikouras, M. Schubert, M. Karl, J. D. Kumar, S. J. Powis, A. di Falco and M. C. Gather, Non-obstructive intracellular nanolasers, *Nat. Commun.*, 2018, **9**, 4817.

14 M. Schubert, K. Volckaert, M. Karl, A. Morton, P. Liehm, G. B. Miles, S. J. Powis and M. C. Gather, Lasing in Live Mitotic and Non-Phagocytic Cells by Efficient Delivery of Microresonators, *Sci. Rep.*, 2017, **7**, 40877.

15 M. Schubert, A. Steude, P. Liehm, N. M. Kronenberg, M. Karl, E. C. Campbell, S. J. Powis and M. C. Gather, Lasing within live cells containing intracellular optical micro-resonators for barcode-type cell tagging and tracking, *Nano Lett.*, 2015, **15**, 5647–5652.

16 Q. Chen, Y.-C. Chen, Z. Zhang, B. Wu, R. Coleman and X. Fan, An integrated microwell array platform for cell lasing analysis, *Lab Chip*, 2017, **17**(16), 2814–2820.

17 Q. Chen, X. Zhang, Y. Sun, M. Ritt, S. Sivaramakrishnan and X. Fan, Highly sensitive fluorescent protein FRET detection using optofluidic lasers, *Lab Chip*, 2013, **13**, 2679–2681.

18 Y. Sun, S. I. Shopova, C.-S. Wu, S. Arnold and X. Fan, Bioinspired optofluidic FRET lasers via DNA scaffolds, *Proc. Natl. Acad. Sci. U. S. A.*, 2010, **107**, 16039–16042.

19 Y.-C. Chen, Q. Chen and X. Fan, Optofluidic chlorophyll lasers, *Lab Chip*, 2016, **16**(12), 2228–2235.

20 X. Li, W. Zhang, W. Y. Wang, X. Wu, Y. Li, X. Tan, D. L. Matera, B. M. Baker, Y. M. Paulus and X. Fan, Optical coherence tomography and fluorescence microscopy dual-modality imaging for in vivo single-cell tracking with nanowire lasers, *Biomed. Opt. Express*, 2020, **11**(7), 3659–3672.

21 X. Wu, Q. Chen, P. Xu, Y.-C. Chen, B. Wu, R. M. Coleman, L. Tong and X. Fan, Nanowire lasers as intracellular probes, *Nanoscale*, 2018, **10**(20), 9729–9735.

22 Z. Gao, W. Zhang, Y. Yan, J. Yi, H. Dong, K. Wang, J. Yao and Y. S. Zhao, Proton-Controlled Organic Microlaser Switch, *ACS Nano*, 2018, **12**, 5734–5740.

23 Q. Chen, M. Ritt, S. Sivaramakrishnan, Y. Sun and X. Fan, Optofluidic lasers with a single molecular layer of gain, *Lab Chip*, 2014, **14**, 4590–4595.

24 V. D. Ta, S. Caixeiro, F. M. Fernandes and R. Sapienza, Microsphere Solid–State Biolasers, *Adv. Opt. Mater.*, 2017, **5**(8), 1601022.

25 M. Humar, A. Dobravec, X. Zhao and S. H. Yun, Biomaterial microlasers implantable in the cornea, skin, and blood, *Optica*, 2017, **4**(9), 1080–1085.

26 X. Li, Y. Qin, X. Tan, Y.-C. Chen, Q. Chen, W.-H. Weng, X. Wang and X. Fan, Ultrasound Modulated Droplet Lasers, *ACS Photonics*, 2019, **6**(2), 531–537.

27 Y. Wang, L. Zhao, A. Xu, L. Wang, L. Zhang, S. Liu, Y. Liu and H. Li, Detecting enzymatic reactions in penicillinase via liquid crystal microdroplet-based pH sensor, *Sens. Actuators, B*, 2018, **258**, 1090–1098.

28 M. Schubert, L. Woolfson, I. R. Barnard, A. M. Dorward, B. Casement, A. Morton, G. B. Robertson, P. L. Appleton, G. B. Miles, C. S. Tucker and M. C. Gather, Monitoring contractility in cardiac tissue with cellular resolution using biointegrated microlasers, *Nat. Photonics*, 2020, 1–7.

29 S. Caixeiro, M. Gaio, B. Marelli, F. G. Omenetto and R. Sapienza, Silk–Based Biocompatible Random Lasing, *Adv. Opt. Mater.*, 2016, **4**(7), 998–1003.

30 A. Fernandez-Bravo, K. Yao, E. S. Barnard, N. J. Borys, E. S. Levy, B. Tian, C. A. Tajon, L. Moretti, M. V. Altoe and S. Aloni, Continuous-wave upconverting nanoparticle microlasers, *Nat. Nanotechnol.*, 2018, 1.

31 Y. Liu, A. Teitelboim, A. Fernandez-Bravo, K. Yao, M. V. P. Altoe, S. Aloni, C. Zhang, B. E. Cohen, P. J. Schuck and E. M. Chan, Controlled Assembly of Upconverting Nanoparticles for Low-Threshold Microlasers and Their Imaging in Scattering Media, *ACS Nano*, 2020, **14**(2), 1508–1519.

32 Z. Yuan, Z. Wang, P. Guan, X. Wu and Y. C. Chen, Lasing–Encoded Microsensor Driven by Interfacial Cavity Resonance Energy Transfer, *Adv. Opt. Mater.*, 2020, **8**(7), 1901596.

33 Y. Huan, S. J. Park, K. C. Gupta, S.-Y. Park and I.-K. Kang, Slide cover glass immobilized liquid crystal microdroplets for sensitive detection of an IgG antigen, *RSC Adv.*, 2017, **7**(60), 37675–37688.

34 I. Verma, S. Sidiq and S. K. Pal, Poly (l-lysine)-coated liquid crystal droplets for sensitive detection of DNA and their applications in controlled release of drug molecules, *ACS Omega*, 2017, **2**(11), 7936–7945.

35 M. Humar, Liquid-crystal-droplet optical microcavities, *Liq. Cryst.*, 2016, **43**(13–15), 1937–1950.

36 C. Wei, S.-Y. Liu, C.-L. Zou, Y. Liu, J. Yao and Y. S. Zhao, Controlled self-assembly of organic composite microdisks for efficient output coupling of whispering-gallery-mode lasers, *J. Am. Chem. Soc.*, 2015, **137**(1), 62–65.

37 M. Sadati, A. I. Apik, J. C. Armas-Perez, J. Martinez-Gonzalez, J. P. Hernandez-Ortiz, N. L. Abbott and J. J. de Pablo, Liquid crystal enabled early stage detection of beta amyloid formation on lipid monolayers, *Adv. Funct. Mater.*, 2015, **25**(38), 6050–6060.

38 S. S. Lee, J. B. Kim, Y. H. Kim and S.-H. Kim, Wavelength-tunable and shape-reconfigurable photonic capsule resonators containing cholesteric liquid crystals, *Sci. Adv.*, 2018, **4**(6), eaat8276.

39 F. F. Xu, Y. J. Li, Y. Lv, H. Dong, X. Lin, K. Wang, J. Yao and Y. S. Zhao, Flat-Panel Laser Displays Based on Liquid Crystal Microlaser Arrays, *CCS Chem.*, 2020, 369–375.